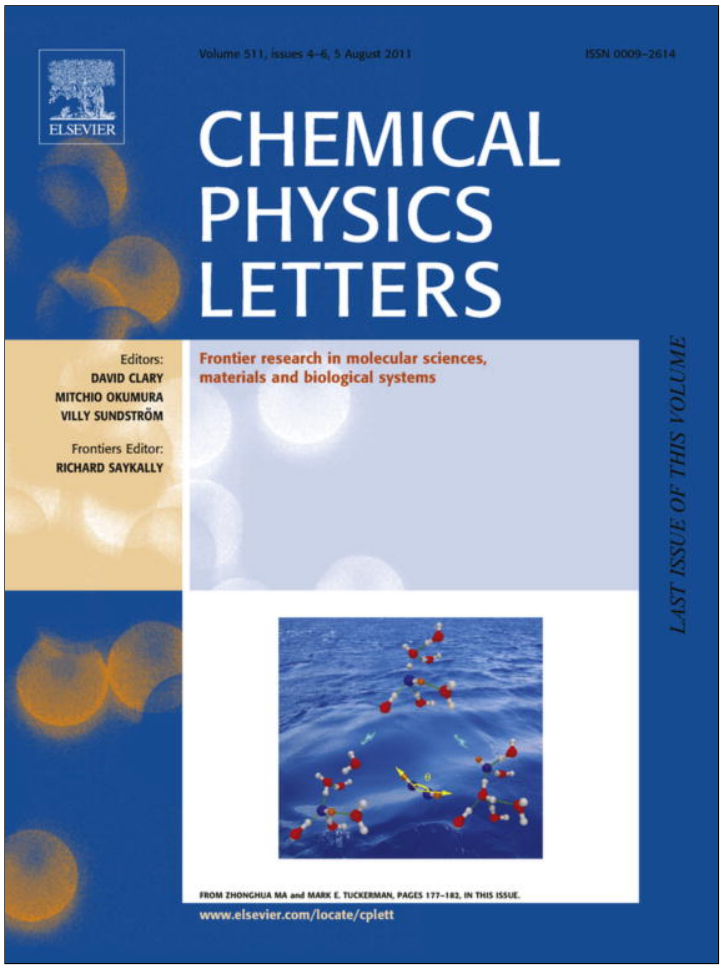

Chemical Physics Letters 511 (2011) 378–383

Contents lists available at ScienceDirect

Chemical Physics Letters

journal homepage: www.elsevier.com/locate/cplett

Spring-block approach for nanobristle patterns

Ferenc Járai-Szabó [a], Emőke-Ágnes Horvát [b], Robert Vajtai [c], Zoltán Néda [a,*]

[a] Faculty of Physics, Babes-Bolyai University, Str. Kogalniceanu Nr. 1, RO-400084 Cluj-Napoca, Romania
[b] Interdisciplinary Center for Scientific Computing, University of Heidelberg, Speyererstr 6, 69115 Heidelberg, Germany
[c] Rice University, Department of Engineering and Material Science, Houston, TX 77005-1827, USA

ARTICLE INFO

Article history:
Received 30 November 2010
In final form 24 June 2011
Available online 29 June 2011

ABSTRACT

A two dimensional spring-block type model is used to model capillarity driven self-organization of nanobristles. The model reveals the role of capillarity and electrostatic forces in the pattern formation mechanism. By taking into account the relevant interactions several type of experimentally observed patterns are qualitatively well reproduced. The model offers the possibility to generate on computer novel nanobristle based structures, offering hints for designing further experiments. In order to allow for experimental validation of the model through future experiments, the cell-size distribution of the simulated cellular pattern is also studied and an exponential form is predicted.

Reproducible nanoscale patterns and structures are of wide interest nowadays for engineering components in modern small-scale electronic, optical and magnetic devices [1]. The so-called *bottom up* approach for the fabrication of these nanostructures uses nanoparticles as elementary building blocks. Under some specific conditions the nanoparticles self-organize into the desired structures [2]. A well-known and widely explored possibility to induce this self-organization is to use the capillarity forces which appear during the drying of a liquid suspension of nanoparticles [3,4]. For instance, regular and irregular two-dimensional polystyrene nanosphere arrays on silica substrates are generated by such methods [5]. These patterns are used then as a convenient mask in the NanoSphere Litography (NSL) method.

Carbon nanotubes (CNT) are attractive materials for nanotechnology because of their interesting physico-chemical properties and molecular symmetries. In order to make them appropriate for certain applications, proper initial CNT configurations have to be built, and specific conditions have to be found which enable their controlled self-organization [6–8]. This is a very ambitious and challenging task, which can be made easier by elaborating working computer models for the self-organization of CNTs on substrates. Therefore, not only experimental, but also computational studies can advance the field of nanoengineering.

In the work of Chakrapani et al. [9] an experimental procedure is presented in which capillary self-organization of nanobristles (or so called 'CNT forrests') leads to puzzling cellular patterns. As pointed out by the authors, crack formation results from the reassembling of highly ordered, elastic CNTs. The obtained remarkable cellular patterns are extraordinarily stable.

The experimental procedure [9] may be shortly summarized as follows. Multi-walled nanotube arrays are grown on rigid silica surface by chemical vapor deposition (CVD) based on the decomposition of ferrocene and xylene. The resulting nanotubes have a wall thickness of ca. 10 nm and a diameter of ca. 30 nm. The average distance between two nanotubes is ca. 50 nm. The obtained nanotube bristle is oxidized in an oxygen plasma at room temperature and 133 Pa pressure for 10 min and immersed in a wetting fluid. After the liquid evaporates, characteristic cellular type patterns are formed as the ends of nanotubes self-organize in compact walls.

Figure 1 shows scanning electron microscope images of some typical structures. From the figures we deduce that a wide variety of structures are engineered in such manner. Both statistically symmetric polygonal cells and rather elongated ones can be obtained by changing the experimental conditions.

These micrometer scale structures have many advantageous features. They can be elastically deformed, transferred to other substrates or used for producing free-standing macroscopic fabrics. Thus, they might find potential applications as shock absorbent reinforcement in nanofiltration devices, elastic membranes and fabrics, and containers for storage or growth of biological cells.

Despite of its applications and the existence of well elaborated production protocols, the exact mechanisms responsible for self-organization of CNTs into vertically aligned cellular structures is not clearly understood. Recently, it has been argued that although we lack some basic information regarding the self-organization of CNTs within a bristle, this process can be approximated with the self-organization of arrays of CNT micropillars of micron-scale diameters [10] each consisting of thousands of CNTs. This observation enables the construction of a computationally tractable model which operates instead of stand-alone CNTs with micropillars.

* Corresponding author. Fax: +40 264 591906.
E-mail address: zneda@phys.ubbcluj.ro (Z. Néda).

0009-2614/$ - see front matter © 2011 Elsevier B.V. All rights reserved.
doi:10.1016/j.cplett.2011.06.068

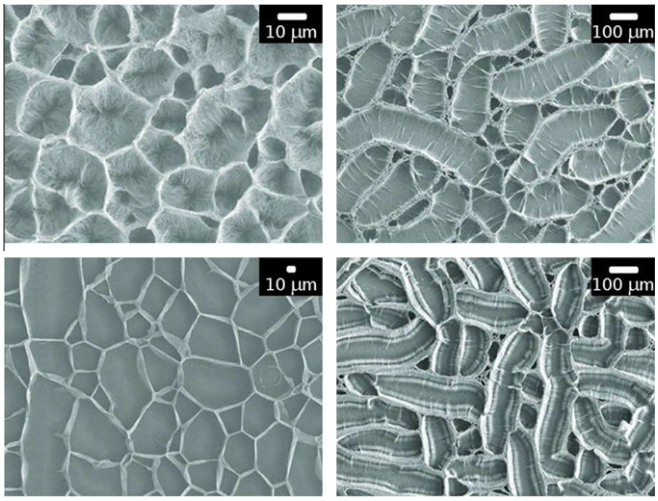

Figure 1. Scanning electron microscope images of the structures obtained in drying nanobristles.

In the present work a simple mechanical spring-block type model defined at mesoscopic micropillar level is considered for understanding the capillarity driven self-organization of nanobristles.

The model is based on the mechanical spring-block stick-slip model family. This model family appeared in 1967, when Burridge and Knopoff [11] constructed a simple mechanical model for explaining the Guttenberg-Richter law for the distribution of earthquakes after their magnitude. The basic elements of the model are blocks and springs that interconnect in a lattice-like topology. The blocks can slide with friction on a planar surface. The original model introduced by Burridge and Knopoff (BK) is one-dimensional. It can be studied numerically and it exhibits self-organized criticality [12]. The BK model gained new perspectives with the strong development of computers and computer simulation methods. Variants of the BK model proved to be useful in describing complex phenomena where avalanche-like processes are present, pattern formation phenomena and mesoscopic processes in solid-state physics or material sciences [13,14].

Recently, by using this model, we have successfully explained the patterns obtained in capillary self-organization of nanospheres [5,16]. Motivated by this success, hereby we propose to map the capillarity driven self-organization of nanotube bristles to a spring-block system, and to understand the pattern selection process by means of computer simulations.

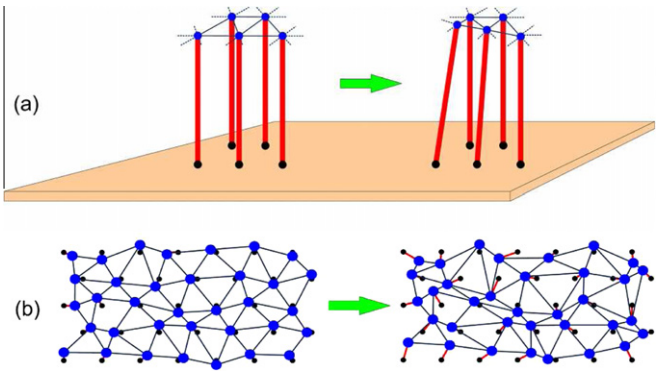

Figure 2. Main elements of the spring-block model. Panel (a) shows a schematic 3D representation of the nanobristle for the initial and a later state. Panel (b) illustrates the dynamics of the equivalent 2D model.

First, let us consider the three-dimensional (3D) model, which is very similar to the real nanotube arrangement. As sketched in Figure 2a, the micropillars composed by thousands of nanotubes having fixed bottom ends are modeled by flexible strands. Their interactions are represented by non-classical springs that connect the neighboring pillars. As motivated below, the evaporation of the liquid is simulated by the stepwise increase of tension in the springs. This will result in the agglomeration of micropillar ends creating the final structure in the studied system.

As shown in Figure 2b, this 3D model can be easily mapped into a two-dimensional (2D) one by projecting the micropillars' top ends on the surface. In the projection plane the micropillars bottom ends are represented as dots, and their positions are fixed on a predefined lattice. The movable top ends are modeled by the disk shaped blocks which can slide with friction on the 2D simulation surface. For visual purposes only, each disk is connected by an extensible string with its bottom end showing the micropillars' trunk. In our simplest approach there is no restriction imposed to the length of these extensible strings which means that nanotubes with infinite length are used. This corresponds to the real case when the nanotubes length is much grater than the linear size of the cells in the final patterns. The disks (top of micropillars) are connected with their nearest neighbors through special springs that model the resulting forces acting between the micropillars.

These special springs are one key ingredient of our computational model. They represent the resultant interaction force acting between two micropillars immersed in suspension. The tension force in the spring has a complex variation with the spring-length, i.e. the inter-pillar distance. It's form is sketched with a red line in the top panel of Figure 3. This force is the resultant of the capillary force, and the dipolar electrostatic repulsion between the micropillars.

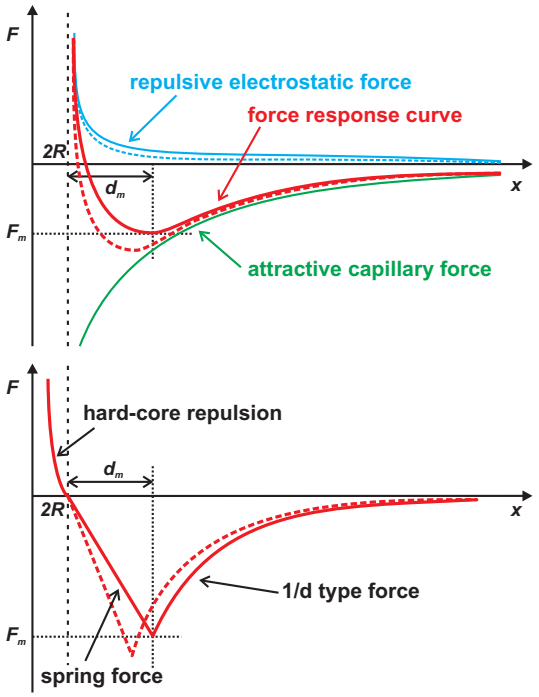

Figure 3. Forces acting between micropillars immersed into liquid (top panel). Forces are shown both at a given time step (solid line), and at a later one (dashed line). The bottom panel shows the length dependence of the net force used for modeling the resultant of the real interactions. It also contains the hard-core repulsion force between disks. Again, the shape of the force curve is shown at an earlier (solid line) and at a later stage (dashed line). The slope of the net force determines the spring-constants.

The capillarity force acting between two micro-scale rods wetted by a liquid was measured experimentally and deduced analytically, too [17–19]. For the analytic form of these forces one might use the formula given in the recent work of Chandra and Yang [20]

$$F_c = -\frac{\pi\gamma R^2 cos^2(\theta)}{\sqrt{\left(\frac{x}{2}\right)^2 - R^2}}, \tag{1}$$

where x is the distance between the centers of the nanotubes, R is the radius of the nanotubes, γ is the liquid–gas surface tension and θ is the contact angle. For $x \gg R$ one gets that this force decays inversely proportionally with the center-to-center distance x.

The repulsive electrostatic force is mainly due to the charge polarization of the nanotubes induced by the hydroxyl radicals that are attached to it as the result of the oxidization process. This dipolar interaction is transmitted through the wetting liquid's molecules (water in our case), which contains polar molecules as well. One can assume, that for $x \gg R$ the strength of this electrostatic repulsion decays as a power-law with the interpillar separation distance $d = x - 2R$ (the dipoles are located on the surface of the nanotube), it is linearly proportional with the dielectric constant (or relative permittivity, ϵ_r) of the medium between the nanotubes and depends also on the average dipolar moment μ per unit length of the nanotubes:

$$F_e = \text{Const} \cdot \frac{\mu^2 \epsilon_r}{d^\alpha} \tag{2}$$

As a first approximation one can consider $\alpha \approx 3$, an exponent which is characteristic for the dipole–dipole interactions. Note that such dipolar repulsive forces between nanotubes immersed in water do appear also without oxidization of the nanotubes [21], but they are important only on smaller length-scales from 0.2 to 1 nm.

The third type of surface forces, attractive van der Waals forces, are important also on this smaller length-scale [21,22], and for interpillar separation distances of tens of nanometers they are one order of magnitude weaker than the capillarity and dipolar electrostatic forces. Thus, we neglect them in our model. The elasticity of the pillars is also not considered due to the large length–diameter ratio of the micropillars. In the studied case, the surface tension is dominant, and thus the bending elasticity looses its relevancy [23,24].

Our model approximates the resultant of the electrostatic repulsion and capillarity attraction forces which reduces to zero for long distances and it has a maximum F_m at distance d_m of micropillars. The special spring-force used in simulations is shown in the bottom panel of Figure 3. For small elongations $d < d_m$ this spring acts as a classical spring with

$$F_k(d) = k(x - 2R) = k \cdot d, \tag{3}$$

where k is the spring constant and $2R$ is its equilibrium length. For elongations longer than d_m the spring force decays as

$$F_k(d) = k'/x, \tag{4}$$

where the constant k' is selected in such way that the force-elongation curve is continuous at d_m.

Similarly with our previous models of drying granular materials [15] or self-organizing nanosphere systems [16], the effects created by the evaporation of the liquid is introduced through these springs. As the liquid evaporates, the water level drops between the nanotubes, leading to a decrease of the effective relative permittivity (ϵ_r) of the medium. As a result, dipolar electric interaction becomes weaker leading to a stronger attractive resultant force. This effect is modeled by a step-by-step increase of the spring constant k. Accordingly, with increasing k the d_m value has to be also proportionally lowered.

The second key ingredient of our spring-block model (necessary to get realistic structures) is the capillary force resulting from the non-vertical orientation of the micropillars. Once the micropillar becomes inclined, the meniscus radius of the liquid surface in contact with the micropillar becomes grater on the side where there is a larger angle between the micropillar and the horizontal surface of the liquid. This leads to an unstable state because a resulting net force $F \sim 1/\cos\Phi$ pointing vertically downwards will act at the crossing point between the liquid surface and the micropillar [23], tending to incline even more the tube. Here we denoted by Φ the angle between the vertical and the tangent to the micropillar at the liquid level. In our spring-block approach this force which is monotonically increasing with the inclination angle is approximated by a simple linear repulsion force

$$F_a(s) = k_a s \tag{5}$$

acting between the disk and its fixed bottom end (s denotes their distance in the simulation plane and k_a is the repulsion constant).

There is an additional almost hard-core–type repulsion F_j which forbids disks to interpenetrate. This is taken into account by the repulsive part of a Lennard–Jones type force which acts only when the distance between two disks becomes smaller than $2R$ (bottom panel of Figure 3).

Additionally to the presented forces, damping forces are considered to stabilize the dynamics. A friction (pinning) between disks and surface is introduced. It can equilibrate a net force less than F_p. Whenever the total force acting on a disk exceeds F_p, the disk slips with an over-damped motion.

The dynamics leading to pattern formation consists of the following relaxation steps. First, the system is initialized. Disks are placed on a triangular lattice with lattice constant a and their corresponding bottom ends are fixed at the same positions. Next, the interconnecting spring-network is build by connecting each disk to its closest neighbors on the lattice. Then, the disks are slightly dislodged in a random direction with a small random shift not grater than the half of the empty space between disks. Thereby, the initial imperfectness of the nanobristle is modeled. The spring constant k is selected in such way that in the initial system the spring forces are not exceeding the pinning force F_p that acts on each disk. An initially pre-stressed spring-block network is thus constructed. During each simulation step the spring constant is increased by a small amount δk representing the increase of tension due to the evaporation of water and the system relaxes to an equilibrium configuration. In this configuration the total net force acting on each disk is lower in magnitude than the pinning threshold F_p.

Similarly with the modelling of drying nanosphere suspensions [16], the relaxation dynamics is realized through an over-damped molecular dynamics simulation using a fixed time-step. The equilibrium state in a viscous medium can be found by moving the disks in each simulation step in the direction of the net force acting on them, and with a displacement which is proportional to the magnitude of the resultant force

$$d\mathbf{r} = \frac{1}{v}\mathbf{F}(\mathbf{r})dt, \tag{6}$$

where v denotes a viscosity. Since the simulation steps will be chosen small enough, this simplified dynamics is able to replace the Newtonian solution without loss of significant information. We remind here that we are not interested in the dynamics, but in the final equilibrium configuration. A relaxation step is finished when no disk slipping event occurs for the given spring constant value. It usually takes a very long time to achieve a perfect relaxation, therefore we introduce a tolerance (10^{-6} to 10^{-9}), and assume that the relaxation is completed when the largest displacement per unit time is smaller than this value. After relaxation is done, we proceed to the next simulation step and increase all spring constants by δk.

This dynamics is repeated until a final, stable configuration of the disks is reached.

When implementing the above relaxation dynamics, several types of boundary conditions can be considered. However, as it was shown in [16] the boundary conditions (free, fixed or periodic) will influence the final stable structure only in the vicinity of boundaries. In the bulk, the obtained structures are rather independent of this choice. Accordingly, in the present simulations fixed boundary conditions are used and snapshots from the bulk are taken for later investigations.

The above presented model has many parameters. In the following we will specify the domains in which they varied during our simulations. On one hand, we identified those parameters that do not influence considerably the resulting patterns. On the other hand, we determined which ones were found to have an impact on the outcome of pattern formation. We use relative (non-dimensional) units. The radius of the nanotubes is taken as unit length. Force unit is fixed by the value of the initial tension in the springs. Simulation steps will define the unit for time, and the unit for viscosity results from Eq. (6).

The disks are considered to have radii $R = 1$, defining the unit length in the system. After fixing the diameter of the circular simulation area $D = 400$–600, the disks are placed on the triangular lattice having a lattice constant $a = 2.2$–5.0. The density (or space filling) of micropillars is implicitly defined by this lattice constant.

The disk sliding dynamics is governed by the viscosity $\nu = 250$ used in Eq. (6) and the pinning threshold $F_p = 0.001$. It was verified by simulations on small sized 200×200 systems that the model will always work for viscosity values selected between reasonable limits $\nu = 100$–1000 and for these viscosity values the final patterns are rather similar (see top row of Figure 4). Choosing a too small viscosity will result in unrealistic oscillations of disks, while a too high value will make disk slips too small and thereby increase considerably the simulation time. Simulations results on small systems reveal the influence of the other parameters as well. The effect of the pinning threshold on the final patterns are presented in the middle line of Figure 4. Based on these results it was concluded that the pinning threshold affects only the number of simulation steps N_0 needed to start the pattern formation process. This may be understood if one takes into account that during simulation spring constants are increased and cell nucleation will start when the net forces acting on tubes is comparable with the pinning threshold.

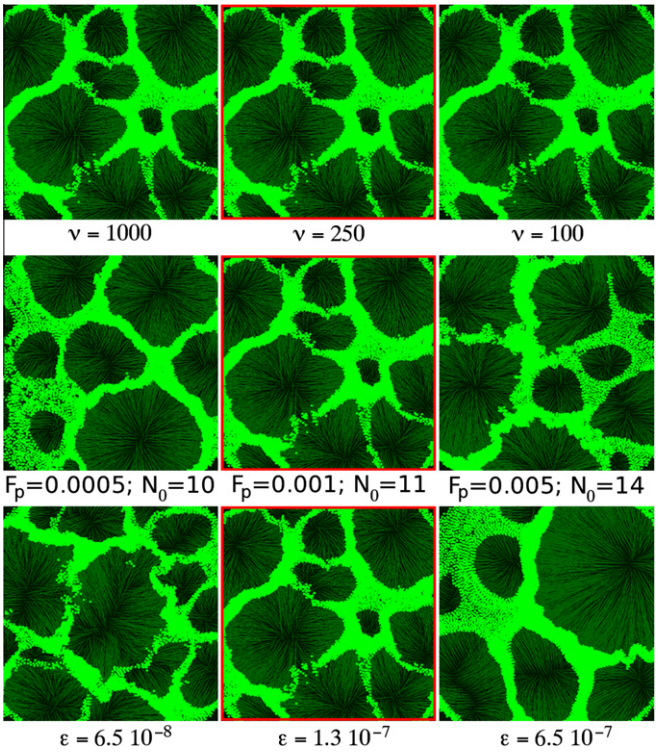

Figure 4. Simulations performed with different viscosity (top), pinning threshold (middle) and Lennard–Jones ε parameter (bottom) values. The parameter values of the red framed panels will be used in large-scale simulations. (For interpretation of the references to color in this figure legend, the reader is referred to the web version of this article.)

The springs used in simulations are characterized by two parameters, namely the initial spring constant $k = 0.01$–0.05 and the equilibrium distance of springs $2R$. By these parameters the non-dimensional unit for the forces in our model system is defined. In order to simulate a quasi-static drying process the spring constant increasing step has to be a small one $\delta k = 0.001$. The central capillary repulsion constant $k_a = 0.0003$ is set to be small enough such as in the initial system, where the micropillars are almost vertical, not to affect the cell formation dynamics. Later, when the walls are forming (and the micropillars are no longer vertically aligned), this force becomes grater and it helps the wall formation and stabilization process.

The used Lennard–Jones force has its standard parameters set to $\sigma = 1.79$ and $\varepsilon = 1.3 \times 10^{-7}$ expressed in simulation units. The value of σ is selected in such way that the minimum of the LJ potential is placed at $x = 2R$. We have performed simulations on systems with small sizes for different ε values. The results are summarized in the bottom row of Figure 4. Based on the visual analysis of the final patterns and the pattern formation dynamics it was concluded that there is no qualitative change of the patterns nor in their formation process in the parameter region $\varepsilon = 6.5 \times 10^{-8} - 3 \times 10^{-7}$. Above this range, some unrealistic oscillations of the nanotubes that are in contact will appear and will dominate the dynamics. This causes that at the beginning of the pattern formation dynamics fewer cells are nucleated and fewer stable walls are formed. Therefore, in the final patterns qualitatively similar but larger cells are obtained. Accordingly, the ε parameter has to be selected from the range, where no unrealistic oscillations are present.

All results presented in the following are obtained with the above chosen parameter values, unless it is otherwise specified in figure captions.

The presented algorithm can be easily implemented and systems up to 300 000 micropillars can be simulated in reasonable computational time. As shown on the time-sequence in Figure 5, the cellular patterns are formed after nucleation of voids in the spring-block network (time step $N = 9$). A preliminary void is enlarged by the tensioned springs (time step $N = 13$) until the top of micropillars arrange in a final and stable cellular structure (time step $N = 16$). The obtained dynamics resembles the pattern formation mechanism known from experimental in-situ observations [9].

Furthermore, the effect of nanotube density on final patterns is computationally investigated. Simulations with the same parameter set are preformed for systems initialized with different lattice constants a. By this, the space filling of the micropillar system

$$\rho = \frac{2\pi}{a^2\sqrt{3}} \tag{7}$$

is varied. Here, it has to be noted that the micropillar density and implicitly the micropillar lattice constant are linearly connected to the real nanotube density ρ_n and the nanotube lattice constant a_n, respectively. If a micropillar is composed by N nanotubes, then by simple geometrical calculations it can be shown that

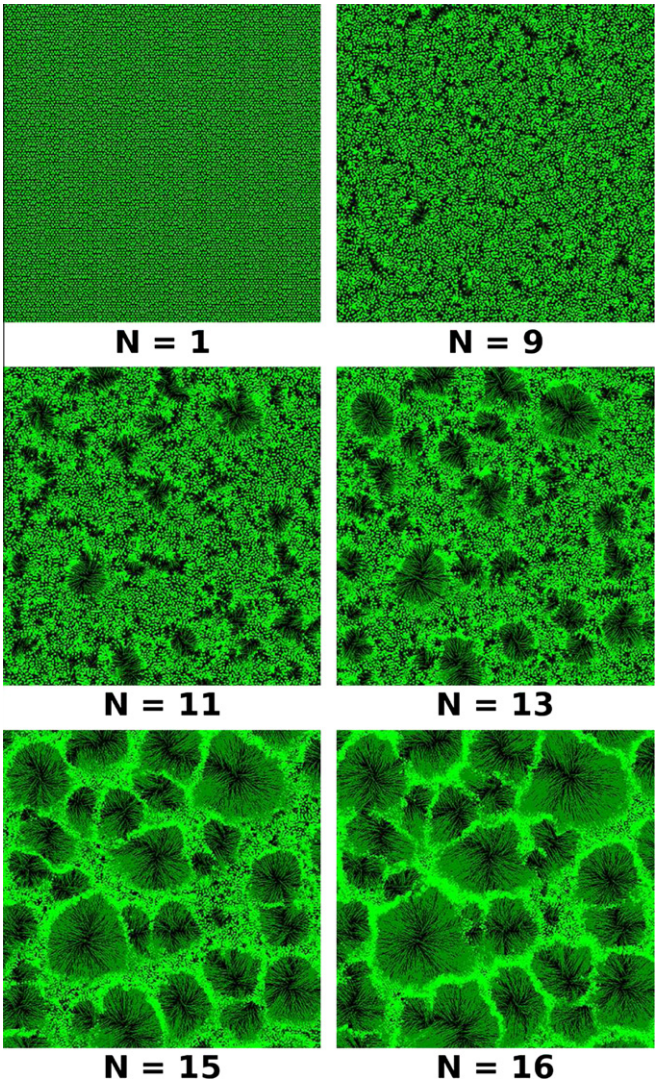

Figure 5. Time evolution of the simulation for parameters $D = 400$, $a = 2.2$ and $k = 0.01$. The simulation time step N is noted below the snapshots.

$$\rho = \rho_n \frac{\pi R^2}{2R_n^2\sqrt{3N}} \text{ and } a = a_n\sqrt{\frac{2\sqrt{3N}}{\pi}}, \tag{8}$$

where R_n denotes the radius of a nanotube.

In Figure 6 three different type of simulated structures are presented. For high space filling $\rho = 0.688$ corresponding to lattice constant $a = 2.4$ (top left panel) polygonal cellular structures are obtained similar to those on the left hand side of Figure 1. As one can observe on the magnified cell image, at the center there is a clean area formed by radially outgoing micropillars. For intermediate space filling $\rho = 0.404$ which corresponds to a lattice constant $a = 3.0$ (top right panel) the micropillars self-organize into elongated cellular structures. The obtained structures are in qualitative agreement with the experimental structures presented in the right hand side SEM images of Figure 1. When interpreting the image, one has to take into account that the length scale of this snapshot is 1.25 times smaller than the length scale of the previously discussed one (top left panel). Accordingly, the typical size of the simulated elongated structures is 3–5 times grater than the typical size of the polygonal structures. For low space filling $\rho = 0.145$ corresponding to a lattice constant $a = 5.0$ (bottom left panel) the micropillars form bundled clusters resembling novel experimental

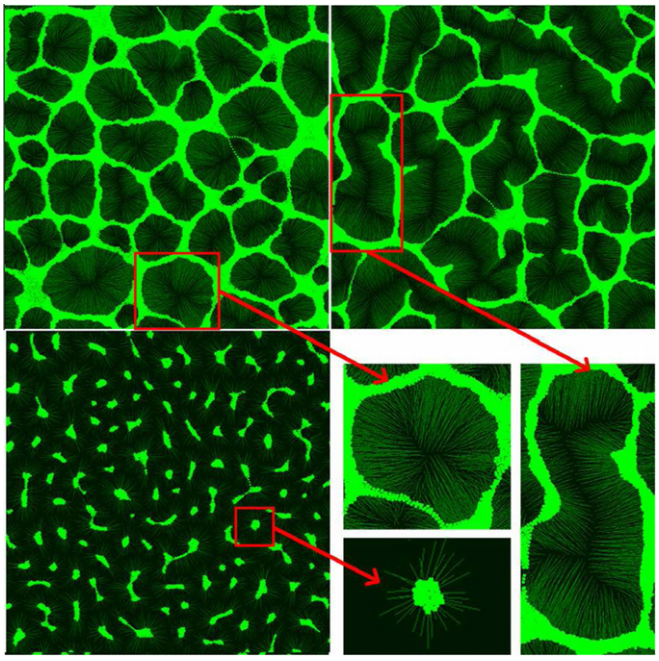

Figure 6. Final structures obtained for various micropillar densities. Simulation results obtain with parameters $D = 600$ and $k = 0.05$. The lattice constant is $a = 2.4$ for the top left panel, $a = 3.0$ for the top right panel and $a = 5.0$ for the bottom left panel. The obtained structures are magnified on the bottom right panel.

patterns of sequential assembly of self-similar nanotube clusters [24].

In order to allow also a quantitative experimental confirmation of the model the cell-size distribution of the simulated pattern is also calculated. The presented results are obtained for the same parameter set as those in Figure 6 except that in this case huge 2000×2000 sized systems are considered. From multiple simulation results 2500 cells are extracted and their size-distribution $f(S)$ is constructed, where S denotes the area of a cell. Instead of $f(S)$ it is more convenient to use the more general $g(y)$ distribution function for the $y = S/\langle S\rangle$ normalized cell sizes. As it is immediately observable from the log-normal representation in Figure 7 the simulated distribution function may be well approximated by an exponential curve.

Finally, our simulations explored also the possibility of designing highly ordered micropatterns in nanobristles. We reconstructed a recent design procedure that is based on the experimental observation that low-density regions or vacancies

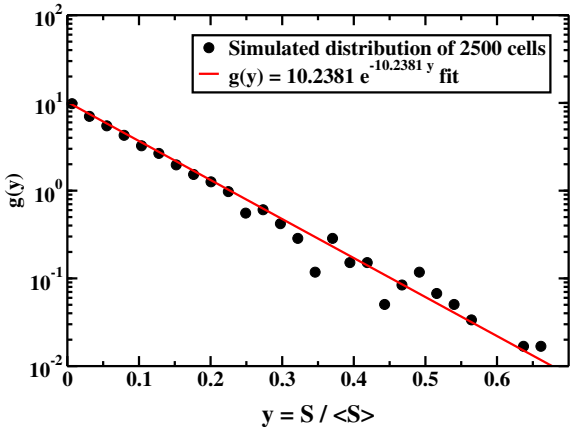

Figure 7. Cell size distribution.

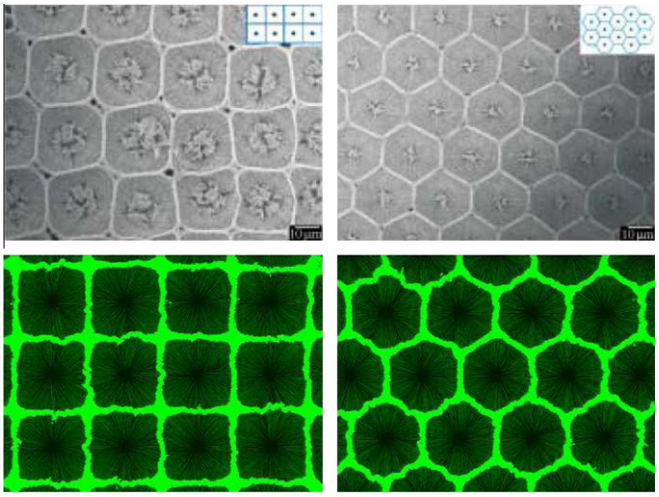

Figure 8. Highly ordered experimentally designed patterns [25] (top) in comparison with simulation results (bottom) for the parameter set $D = 600$, $a = 2.6$ and $k = 0.01$.

in the bristle play an important role in the cellular pattern nucleation process [25]. As shown in top panels of Figure 8, different kinds of highly ordered micropatterned structures have been created by etching regular vacancies with laser pulses. Capillary self-organization in such systems yields the structures presented on the top panels of Figure 8.

Simulations on micropillar forests with vacancies of radius $r = 5$ created on rectangular and triangular lattices have been performed. The results are shown on bottom panels of Figure 8. In agreement with experimental findings, our spring-block simulation results suggest that various micropatterns may be designed by proper preparation of the initial nanobristle taking into account that the wall of a polygon shaped cell forms approximately at the vertical bisector of two adjacent vacancies.

In conclusion, a simple mechanical, spring-block type model has been proposed here to model capillarity driven self-organization of nanobristles. The 3D problem was mapped to a 2D model that works at the mesoscopic micropillar level incorporating real interactions known from earlier experimental studies. Our computer simulations evidenced the role of capillary and electrostatic forces in the formation of self-organized nanostructures. The dynamics leading to pattern formation has been also revealed. By using the same model parameters with different nanotube densities three qualitatively different types of patterns were reproduced. Large-scale simulations revealed an exponential distribution of cell sizes for the polygonal type final patterns. The obtained exponential distribution is interesting from two aspects. First, it gives a possibility to experimentally test our model, and secondly it suggests that the dynamics in the system leads to a maximum entropy distribution. Considering a fixed area and fixed number of cells (fixed average cell size), the exponential distribution of cell sizes is the entropy maximizing distribution [26]. As a further challenge for experimentalists and test for the elaborated model, the possibility of designing highly ordered nanostructures has also been explored.

Acknowledgements

This work was supported by Grants PN II-IDEI 2369/2008 and PNII/ID/PCCE:312/2008. One of the authors (EÁH) was partly funded by a scholarship from the Heidelberg Graduate School of Mathematical and Computational Methods for the Sciences, University of Heidelberg, Germany, which is funded by the German Excellence Initiative (GSC 220).

References

[1] M. Rieth, Nano-Engineering in Science and Technology: An Introduction to the World of Nano-Design (Series on the Foundations of Natural Science and Technology), World Scientific Publishing Co., Inc., New York, 2003.
[2] M. Adachi, D.J. Lockwood (Eds.), Self-Organized Nanoscale Materials, Springer, New York, 2006.
[3] Ch. L. Haynes, R.P. van Duyne, J. Phys. Chem. B 105 (2001) 5599.
[4] A.A. Chabanov, Y. Jun, D.J. Norris, Appl. Phys. Lett. 84 (2004) 3573.
[5] F. Járai-Szabó, Z. Néda, S. Aştilean, C. Farcau, A. Kuttesch, Eur. Phys. J. E. 23 (2007) 153.
[6] F. Ding, K. Jiao, Y. Lin, B.I. Yakobson, Nano Lett. 7 (2007) 681.
[7] D.P. Young et al., J. Appl. Phys. 103 (2008) 053503.
[8] E.R. Meshot et al., ACS Nano 3 (2009) 2477.
[9] N. Chakrapani et al., Proc. Natl. Acad. Sci. 101 (2004) 4009.
[10] M.F.L. De Volder, D.O. Vidaud, E.R. Meshot, S. Tawfick, A.J. Hart, Microelectron. Eng. 87 (2010) 1233.
[11] R. Burridge, L. Knopoff, Bull. Seism. Soc. Am. 57 (1967) 341.
[12] P. Bak, How Nature Works: The science of Self-Organized Criticality, Copernicus, New York, 1996.
[13] J.V. Andersen, Y. Brchet, H.J. Jensen, Europhys. Lett. 26 (1994) 13.
[14] K. Kovács, Y. Brechet, Z. Néda, Modell. Simul. Mater. Sci. Eng. 13 (2005) 1341.
[15] K.-t. Leung, Z. Néda, Phys. Rev. Lett. 85 (2000) 662.
[16] F. Járai-Szabó, S. Aştilean, Z. Néda, Chem. Phys. Lett. 408 (2005) 241.
[17] C.D. Dushkin, P.A. Kralchevsky, H. Yoshimura, K. Nagayama, Phys. Rev. Lett. 75 (1995) 3454.
[18] P.A. Kralchevsky, V.N. Paunov, I.B. Ivanov, K. Nagayamam, J. Colloid Interface Sci. 151 (1992) 79.
[19] G. Kaptay, J. Mat. Sci. 40 (2005) 2125.
[20] D. Chandra, S. Yang, Langmuir 25 (2009) 10430.
[21] L. Li, D. Bedrov, G.D. Smith, J. Phys. Chem. 110 (2006) 10509.
[22] N.M. Uddin, F. Capaldi, B. Farouk, J. Eng. Mat. Tech. 132 (2010) 021012.
[23] S. Neukirch, B. Roman, B. de Gaudemaris, J. Bico, J. Mech. Phys. Solids 55 (2007) 1212.
[24] B. Pokroy, S.H. Kang, L. Mahadevan, J. Aizenberg, Science 323 (2009) 237.
[25] H. Liu, S. Li, J. Zhai, H. Li, Q. Zheng, L. Jiang, D. Zhu, Angew. Chem. Int. Ed. 43 (2004) 1146.
[26] E.T. Jaynes, Phys. Rev. 106 (1957) 620.